PROCEEDINGS OF SCIENCE

The r-process – the theoretical/astrophysical side

Shinya Wanajo[*1,2], **Hans-Thomas Janka**[2], **and Bernhard Müller**[2]

[1] *Technische Universität München, Excellence Cluster Universe, Boltzmannstr. 2, D-85748 Garching, Germany*

[2] *Max-Planck-Institut für Astrophysik, Karl-Schwarzschild-Str. 1, D-85748 Garching, Germany*

E-mail: shinya.wanajo@universe-cluster.de

All the current r-process scenarios relevant to core-collapse supernovae are facing severe difficulties. In particular, recent core-collapse simulations with neutrino transport show no sign of a neutron-rich wind from the proto-neutron star. Recent one-dimensional (1D) hydrodynamical simulations of core-collapse supernovae (CCSNe) with a sophisticated treatment of neutrino transport indicate the neutrino-driven winds being proton-rich all the way until the end of their activity. New 2D explosion simulations of electron-capture supernovae (ECSNe; a subset of CCSNe) exhibit, however, convective neutron-rich lumps, which are absent in the 1D case. Our nucleosynthesis calculations indicate that these neutron-rich lumps allow for interesting production of elements between iron group and $N = 50$ nuclei (from Zn to Zr, with little Ga). Our models do not confirm, however, ECSNe as sources of the strong r-process (but possibly of a weak r-process up to Pd, Ag, and Cd in the neutron-rich lumps). We further discuss nucleosynthesis of the r-process in an alternative astrophysical site, "black hole winds", the neutrino-driven outflows from the accretion torus around a black hole. This condition is assumed to be realized in double neutron star mergers, neutron star – black hole mergers, or hypernovae, but we argue that conditions for strong r-processing are more likely to be realized in the merger case.

11th Symposium on Nuclei in the Cosmos, NIC XI
July 19-23, 2010
Heidelberg, Germany

[*] Speaker.

PoS(NIC XI)079

1. Introduction

In the past decades, core-collapse supernovae have been considered to be the most promising astrophysical site that provides the suitable conditions for nucleosynthesis of the r-process. The scenarios include the neutrino-driven wind [1, 2, 3, 4, 5, 6], the prompt explosion of a collapsing oxygen-neon-magnesium (O-Ne-Mg) core [7], and the shocked surface layer of an O-Ne-Mg core [8]. However, recent one-dimensional (1D) hydrodynamical simulations of an collapsing O-Ne-Mg core do not support the prompt explosion [9] or the shocked surface layer [10] scenarios. The nucleosynthesis calculations [11, 12] with these hydrodynamical results also show that the production of neutron-capture elements proceeds only up to $A = 90$ ($N = 50$). Furthermore, recent long-term simulations of core-collapse supernovae show that the neutrino-driven outflows are proton-rich all the way [13], which poses a severe difficulty to all the scenarios relevant to the neutrino-driven winds of core-collapse supernovae.

Multi-dimensionality changes the above situation for the early neutrino-driven ejecta. New self-consistent 2D explosion simulations of electron-capture supernovae (ECSNe; a subset of CCSNe arising from collapsing O-Ne-Mg cores) exhibit n(eutron)-rich lumps of matter being dredged up by convective overturn from the outer layers of the PNS during the early stages of the explosion (Müller, Janka, & Kitaura, in preparation), a feature that is absent in the 1D situation. This allows for interesting production of elements beyond iron in nuclear statistical equilibrium (NSE), by α-processing, and potentially by weak r-processing [14].

Another popular scenario of the astrophysical r-process, the mergers of double neutron stars (NS-NS) [15] or of a black hole and a neutron star (BH-NS) [16] in a close binary system, has not been fully explored so far. The decomposition of cold unshocked neutron-rich matter from NS-NS is suggested to be an alternative or additional r-process site [17, 18, 19, 20]. In addition, both NS-NS and BH-NS are expected to form an accretion torus around a black hole, giving rise to the neutrino-driven winds ("black hole winds"), which are also expected to provide suitable physical conditions for the r-process [21]. In fact, some recent studies of Galactic chemical evolution based on the hierarchical clustering of sub-halos [23] do not exclude the mergers as the dominant astrophysical site of the r-process (see also [24]).

In this article, we outline our recent results of nucleosynthesis studies on the basis of self-consistent 2D models of ECSNe [14], aiming at identifying the origins of nuclei beyond iron. The sensitivity of the nucleosynthetic yields on the minimum $Y_{\rm e}$ (electron fraction or the number of protons per baryon) in n-rich lumps, $Y_{\rm e,min}$, is also examined to investigate whether ECSNe can lead to an r-process. We further examine the r-process in black hole winds, which are common both in NS-NS and BH-NS mergers, and presumably, in "collapsars". Currently, however, three-dimensional simulations of the mergers are out of reach for the wind phase after the formation of a stable accretion torus [15, 16]. Hence, we apply the semi-analytic wind model for nucleosynthesis calculations [5].

2. Nucleosynthesis in the early ejecta of Electron-capture Supernovae

The nucleosynthesis analysis made use of about 2000 representative tracer particles, by which the thermodynamic histories of ejecta chunks were followed in our 2D hydrodynamic calculation of

an ECSN. The model was computed with a sophisticated (ray-by-ray-plus) treatment of the energy-dependent neutrino transport, using the PROMETHEUS-VERTEX code and the same microphysics (weak-interaction rates, nuclear burning treatment, and nuclear equation of state of [25]) as in its 1D counterpart [9]. Some aspects of the 2D model in comparison to 1D results were discussed by [10].

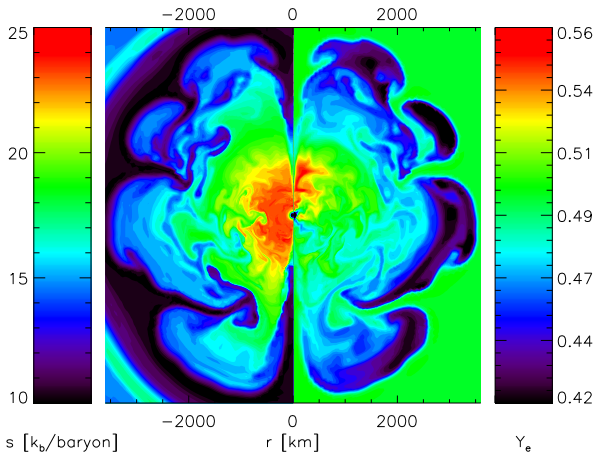

Figure 1: Snapshot of the convective region of the 2D simulation of an ECSN at 262 ms after core bounce with entropy per nucleon (s; left) and Y_e (right).

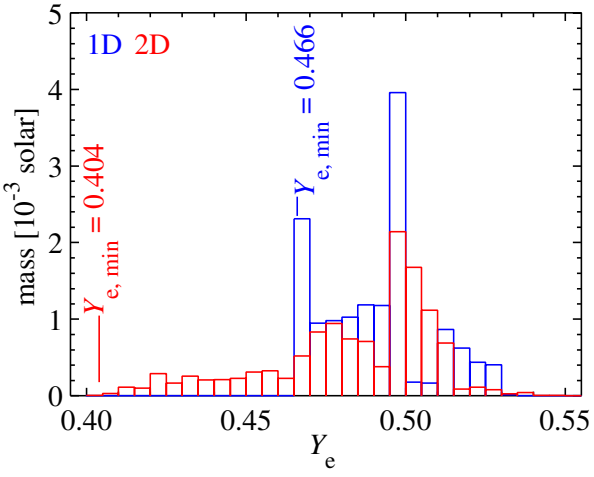

Figure 2: Ejecta masses vs. Y_e for the 1D (blue) and 2D (red) explosion models. The width of a Y_e-bin is chosen to be $\Delta Y_e = 0.005$.

The pre-collapse model of the O-Ne-Mg core emerged from the evolution of an $8.8\,M_\odot$ star [26]. Because of the very steep density gradient near the core surface, the shock expands continuously, and a neutrino-powered explosion sets in at $t \sim 100$ ms p.b. in 1D and 2D essentially in the same way and with a very similar energy ($\sim 10^{50}$ erg) [10].

In the multi-dimensional case, however, the negative entropy profile created by neutrino heating around the PNS leads to a short phase of convective overturn, in which accretion downflows deleptonize strongly, are neutrino heated near the neutrinosphere, and rise again quickly, accelerated by buoyancy forces. Thus n-rich matter with modest entropies per nucleon ($s \sim 13$–$15\,k_B$; k_B is Boltzmann's constant) gets ejected in mushroom-shaped structures typical of Rayleigh-Taylor instability. Figure 1 displays the situation 262 ms after bounce when the pattern is frozen in and self-similarly expanding.

As a consequence, the mass distribution of the ejecta in the 2D model extends down to $Y_{e,min}$ as low as $\sim$0.4, which is significantly more n-rich than in the corresponding 1D case ($Y^{1D}_{e,min} \sim 0.47$). Figure 2 shows the Y_e-histograms at the end of the simulations. The total ejecta masses are $1.39 \times 10^{-2}\,M_\odot$ for the 1D model and $1.14 \times 10^{-2}\,M_\odot$ in 2D, where the difference is partly due to the different simulation times, being $\sim$800 ms and $\sim$400 ms, respectively (core bounce occurs at $\sim$50 ms). However, the ejecta after $\sim$250 ms p.b. are only proton-rich, contributing merely to the $Y_e > 0.5$ side in Fig. 2.

The nucleosynthetic yields are obtained with the reaction network code (including neutrino interactions) described in [12]. Using thermodynamic trajectories directly from the 2D ECSN model, the calculations are started when the temperature decreases to 9×10^9 K, assuming initially

free protons and neutrons with mass fractions Y_e and $1-Y_e$, respectively. The final abundances for all isotopes are obtained by mass-integration over all 2000 marker particles.

The resulting *elemental* mass fractions relative to solar values, or the production factors, are shown in Fig. 3 (red) compared to the 1D case (blue) from [12]. The "normalization band" between the maximum (367 for Sr) and a tenth of that is indicated in yellow with the medium marked by a dotted line. The total ejecta mass is taken to be the sum of the ejected mass from the core and the outer H/He-envelope ($=8.8M_\odot-1.38M_\odot+0.0114M_\odot=7.43M_\odot$). Note that the $N=50$ species, ^{86}Kr, ^{87}Rb, ^{88}Sr, and ^{90}Zr, have the largest production factors for *isotopes* with values of 610, 414, 442, and 564, respectively.

As discussed by [12], in the 1D case only Zn and Zr are on the normalization band, although some light p-nuclei (up to ^{92}Mo) can be sizably produced. In contrast, we find that all elements between Zn and Zr, except for Ga, fall into this band in the 2D case (Ge is marginal), although all others are almost equally produced in 1D and 2D. This suggests ECSNe to be likely sources of Zn, Ge, As, Se, Br, Kr, Rb, Sr, Y, and Zr, in the Galaxy. Note that the origin of these elements is not fully understood, although Sr, Y, and Zr in the solar system are considered to be dominantly made by the s-process. The ejected masses of ^{56}Ni ($\rightarrow^{56}$Fe; $3.0\times10^{-3}M_\odot$) and all Fe ($3.1\times10^{-3}M_\odot$) are the same as in the 1D case ($2.5\times10^{-3}M_\odot$) [12].

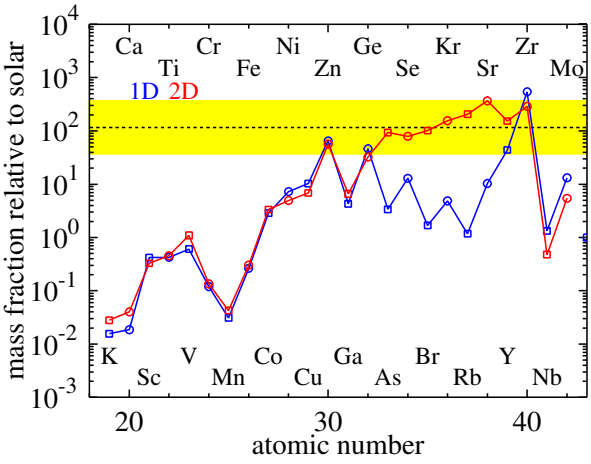

Figure 3: Elemental mass fractions in the ECSN ejecta relative to solar values, comparing the 2D results (red) with the 1D counterpart (blue) from [12]. The normalization band (see text) is marked in yellow.

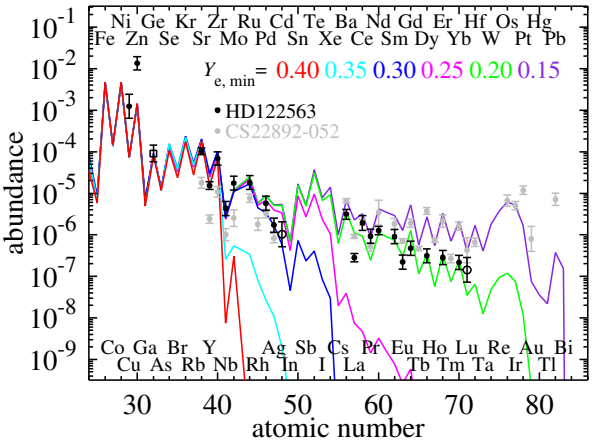

Figure 4: Elemental abundances for various $Y_{e,min}$ compared with the stellar abundances of the r-process deficient star HD 122563 with [Fe/H]≈-2.7 [27, 29, 30] and the r-process enhanced star CS 22892-052 with [Fe/H]≈-3.1 [31].

The fact that oxygen is absent in ECSN ejecta but a dominant product of more massive CCSNe, can pose a constraint on the frequency of ECSNe [12]. Considering the isotope ^{86}Kr with its largest production factor in our 2D model and assuming f to be the fraction of ECSNe relative to all CCSNe, one gets

$$\frac{f}{1-f}=\frac{X_\odot(^{86}\mathrm{Kr})/X_\odot(^{16}\mathrm{O})}{M(^{86}\mathrm{Kr})/M_{\mathrm{noEC}}(^{16}\mathrm{O})}=0.050, \tag{2.1}$$

where $X_\odot(^{86}\mathrm{Kr})=2.4\times10^{-8}$ and $X_\odot(^{16}\mathrm{O})=6.6\times10^{-3}$ are the mass fractions in the solar system, $M(^{86}\mathrm{Kr})=1.1\times10^{-4}M_\odot$ is our ejecta mass of ^{86}Kr, and $M_{\mathrm{noEC}}(^{16}\mathrm{O})=1.5M_\odot$ the production of

^{16}O by all other CCSNe, averaged over the stellar initial mass function between $13\,M_\odot$ and $40\,M_\odot$ (see [12]). Equation (1) leads to $f = 0.048$. The frequency of ECSNe relative to all CCSNe is thus ∼4%, assuming that all ^{86}Kr in the solar system except for a possible contribution from the s-process (∼ 20%), originates from ECSNe. This is in good agreement with the prediction from a recent synthetic model of super asymptotic-giant-branch stars (for solar metallicity models, [32]).

The remarkable difference between the 1D and 2D cases (Fig. 3) can be understood by the combined element formation in nuclear statistical equilibrium (NSE) and through the α-process (or "n-rich, α-rich freezeout from NSE", [33]). The α-process makes nuclei heavier than the Fe-group up to $A \sim 100$. ^{64}Zn, ^{88}Sr, and ^{90}Zr are thus produced at $Y_\mathrm{e} = 0.43$–0.49. The α-process, however, is known to leave a deep trough in the abundance curve between A ∼60 and 90 because of the strong binding at $N = 28$ and 50. This explains the substantial underproduction of elements around Z ∼33–37 in the 1D case (Fig. 3, blue line).

Since NSE with neutron excess ($Y_\mathrm{e} \sim 0.4$) leads to nuclei heavier than the Fe-group up to $A \approx 84$ (see, e.g., [34]), the trough can be filled by NSE-abundances assembled in the n-rich ejecta lumps. Accordingly, NSE in the Y_e-range of 0.40–0.42 yields substantial amounts of species with $A = 74$–84, nuclei that cannot be created by the α-process.

In the n-rich ejecta lumps NSE-like conditions are established for several reasons. They have smaller entropies ($s \approx 13$–$15\,k_\mathrm{B}$ per baryon) than the other ejecta (where $s \approx 15$–$20\,k_\mathrm{B}$ per baryon; Fig. 1). This favors α-particles to disappear when NSE ends as the temperature drops. In addition, the α's become easily locked up and tightly bound in nuclei, i.e., their separation energies are large (cf., e.g., Fig. 1b in [33]), because nuclei with n-excess do not readily release α's to move farther away from β-stability.

Our results also imply that ECSNe can be the source of Sr, Y, and Zr as observed in r-process deficient Galactic halo stars (Fig. 4). A number of such stars with detailed abundance determinations indicate, however, a possible link with the elements beyond $N = 50$, e.g. Pd and Ag [27]. Our ECSN models cannot account for the production of such elements, but in their ejecta a small change of Y_e can drastically change the nucleosynthesis [12]. Due to limitations of the numerical resolution and the lack of the third dimension, or some sensitivity to the nuclear equation of state, it cannot be excluded that ECSNe also eject tiny amounts of matter with $Y_\mathrm{e,min}$ slightly lower than predicted by the 2D simulation.

We therefore compare the nucleosynthesis for $Y_\mathrm{e,min} = 0.40$ of our ECSN model and for artificially reduced values of $Y_\mathrm{e,min} = 0.35, 0.30, 0.25, 0.20$, and 0.15 with the abundance patterns of representative r-process deficient (HD 122563, [27, 29, 30]) and enhanced (CS 22892-052, [31]) stars (Fig. 4). For that we use the thermodynamic trajectory of the lowest Y_e ($= 0.404$) of the original model but apply Y_e down to 0.15 in steps of $\Delta Y_\mathrm{e} = 0.005$. The ejecta masses in these additional Y_e-bins are chosen to be constant with $\Delta M = 2 \times 10^{-5}\,M_\odot$ in the cases $Y_\mathrm{e,min} = 0.35$ and 0.30, and $\Delta M = 10^{-5}\,M_\odot$ for the other $Y_\mathrm{e,min}$.

Figure 4 shows that $Y_\mathrm{e} \leq 0.35$ is needed to obtain elements beyond $N = 50$. A remarkable agreement with the abundance pattern in HD 122563 up to Cd ($Z = 48$) can be seen for $Y_\mathrm{e,min} = 0.30$. Such a mild reduction of $Y_\mathrm{e,min}$ in the ECSN ejecta is well possible for the reasons mentioned above. A reasonable match of the heavier part beyond $Z = 48$ requires $Y_\mathrm{e,min} \approx 0.20$. This, however, leads to a poor agreement for Ag and Cd. We therefore speculate that ECSNe could be the sources of the elements up to Cd in r-process deficient stars, and the heavier elements are

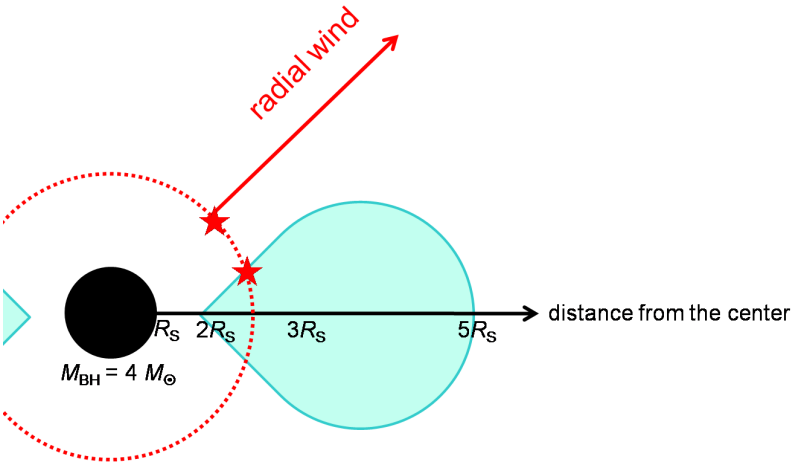

Figure 5: Sketch of our model settings for the black hole winds. A rotating black hole with the mass $M_{\rm BH} = 4M_\odot$ is located in the center of an accretion torus ("neutrino surface") that lies between $2R_{\rm S}$ and $5R_{\rm S}$ from the center, where $R_{\rm S}$ is the Schwarzschild radius ($= 11.8$ km). The wind is assumed to be radial, where the neutrino surface is replaced with an equivalent radius from the center (e.g., the star on the dotted circle).

from a different origin. Moreover, $Y_{\rm e,min} = 0.15$ is necessary to reproduce the abundance pattern of r-process enhanced stars like CS 22892-052. Such a low $Y_{\rm e}$ seems out of reach and disfavors ECSNe as production sites of heavy r-process nuclei.

We note that the neutron-capture reactions start from seeds with $A \sim 80$ formed in NSE-like conditions, not from the α-processed seeds ($A \sim 90$–100). We therefore prefer to call the described process producing the elements beyond $N = 50$, presumably up to Cd, "weak r-process" [35, 27] rather than α-process or charged-particle process [33].

Our present calculations are limited to the first $\lesssim$400 ms after bounce and do not include the neutrino-driven PNS wind. The latter, however, turned out to have proton excess in 1D models of the long-term evolution of ECSNe [13]. It thus makes only p-rich isotopes as discussed in § 3 and has no effect on the discussed results in this section.

3. Nucleosynthesis in the Black Hole Winds

Our model of black hole winds is based on the semi-analytic, spherically symmetric, general relativistic model of proto-neutron star winds [5], as illustrated in Figure 5. The mass of a central black hole is taken to be $M_{\rm BH} = 4M_\odot$, which may correspond to, e.g., NS-NS binaries with the equal masses of $\sim 2M_\odot$ or BH-NS binaries with the masses of $\sim 2.5M_\odot$ and $\sim 1.5M_\odot$. This can be also interpreted as the accreting black hole of the collapsar from a massive ($> 30M_\odot$) progenitor. The accretion torus around the black hole, which is defined as the "neutrino surface", is assumed to lie between $2R_{\rm S}$ ($= 23.6$ km) and $5R_{\rm S}$ ($= 35.4$ km) from the center (where $R_{\rm S}$ is the Schwarzschild radius $= 11.8$ km) in the light of detailed hydrodynamical simulations of BH-NS merging [16].

In order to connect the aspherical configuration of the winds from the torus to our spherical model, an arbitrary point on the torus is replaced by a point on the hypothetical neutrino sphere with an equal distance from the center, R_ν (dotted circle in Figure 5). The solution of the wind from

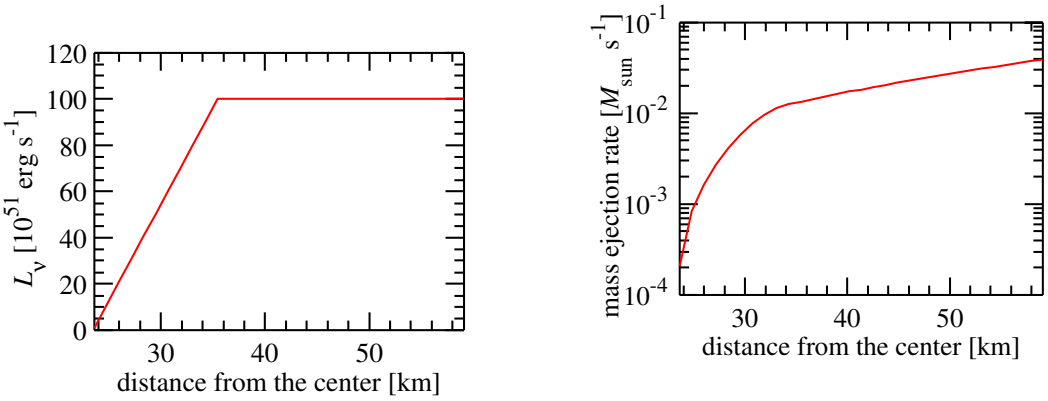

Figure 6: Left: Neutrino luminosity L_ν as a function of the distance from the center. L_ν is assumed to increase linearly from 10^{51} erg s^{-1} to 10^{53} erg s^{-1} between $2R_S$ ($= 23.6$ km) and $3R_S$ ($= 35.4$ km) and take a constant value on the outer side. Right: Mass ejection rate $\dot{M}$ obtained with the L_ν profile assumed in the left panel, as a function of the distance from the center.

the neutrino sphere with M_{BH} and R_ν is then obtained in the same manner as for proto-neutron star winds. The rms average neutrino energies are taken to be 15, 20, and 30 MeV, for electron, anti-electron, and the other flavors of neutrinos, respectively [16]. The neutrino luminosities of all the flavors are assumed to be the same value L_ν. The mass ejection rate at the neutrino sphere $\dot{M}$ is determined so that the wind becomes supersonic through the sonic point.

As anticipated from Figure 5, the neutrino flux from the outer regions of the torus is shielded in the vicinity of the black hole by the presence of the torus itself. In order to mimic this effect in our spherical models, we simply assume that L_ν increases linearly from 10^{51} erg s^{-1} to 10^{53} erg s^{-1} between $2R_S$ ($= 23.6$ km) and $3R_S$ ($= 35.4$ km) and takes a constant value on the outer side, as shown in Figure 6 (left panel). This roughly reproduces the peak energy deposition rate by $\nu\bar{\nu}$ annihilation into e^+e^- pairs in the vicinity of the black hole ($\sim 10^{30}$ erg s^{-1} cm^{-3}) [15, 16]. We define the outflows from $R_\nu < 3R_S$ and $R_\nu > 3R_S$ as the inner and outer winds, respectively.

As shown in Figure 6 (right panel), inner winds have rather small $\dot{M}$ owing to the small L_ν at R_ν. As a result, the inner winds obtain substantially higher asymptotic entropies (at 0.5 MeV, up to $\sim 800k_B$ per nucleon, where k_B is the Boltzmann constant; Figure 7, left panel) and short expansion timescales (defined as the e-folding time of temperature from 0.5 MeV, down to ~ 1 ms; Figure 7, right panel). This is due to the larger heating rate *per unit mass* by $\nu\bar{\nu}$ annihilation *after* leaving the neutrino surface, owing to the smaller matter density in the inner wind (see the same effect in anisotropic proto-neutron star winds in [28]). This indicates that the inner winds are favored for the strong r-process (see speculations in [15]).

The initial compositions are then given by the initial electron fraction Y_{e0} (number of protons per nucleon). In this study, Y_{e0} is taken to be a free parameter. We explore the nucleosynthesis for all the winds with $Y_{e0} = 0.10, 0.15, 0.20, 0.25, 0.30$, which are consistent with a recent hydrodynamic

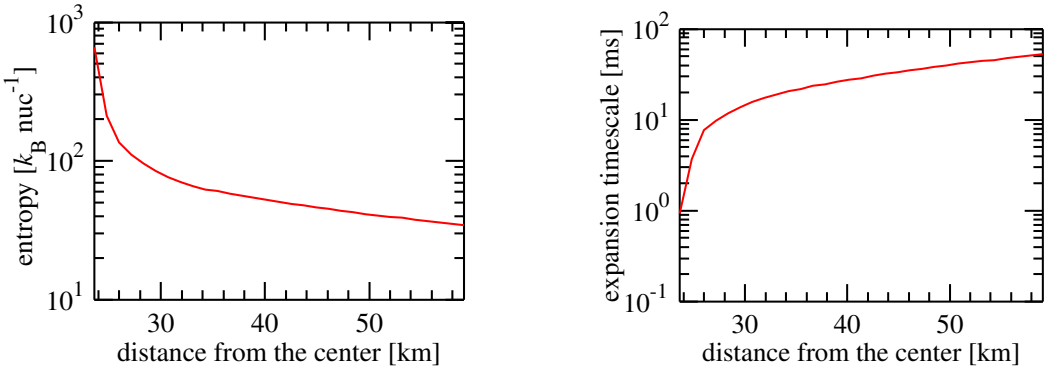

Figure 7: Left: Asymptotic entropy (at 0.5 MeV) as a function of the distance from the center. Right: Expansion timescale (the *e*-folding time of temperature from 0.5 MeV) as a function of the distance from the center.

study of BH-NS [21]. Note that the initial Y_e in the torus, consisting of decompressed NS matter is low, and Y_e in the outgoing wind remains to be low because $L_{\bar{\nu}_e} > L_{\nu_e}$ for the torus during a significant time of its evolution (e.g., [22]).

The neutron-to-seed ratios at the onset of r-processing (defined at 2.5×10^9 K) are shown in Figure 8 (left panel). Note that Y_e at this stage is ~ 0.1 higher than Y_{e0} owing to the neutrino effects, which is obviously overestimated in our assumption of $L_{\bar{\nu}_e} = L_{\nu_e}$. In all the Y_{e0} cases, the neutron-to-seed ratios are substantially higher than 100 (that is required for the 3rd r-process peak formation) in the innermost winds owing to the high entropies and the short expansion timescales (Figure 7), where the fission cycling is expected. In the outer winds, however, only the low Y_{e0} case attains a high neutron-to-seed ratio (up to ~ 70) because of the moderate entropies and expansion timescales.

For each Y_{e0} case, the nucleosynthetic yields are mass-averaged over the entire range of R_ν (from $2R_S$ to $5R_S$), which is shown in Figure 8 (right panel). Despite the high neutron-to-seed ratios in the inner winds, the $Y_{e0} = 0.25$ and 0.30 cases contribute only up to the 2nd r-process peak ($A = 130$) because of the very small $\dot{M}$ in the inner winds (Figure 6, right panel). Our result indicates that neutron-rich winds with $Y_{e0} < 0.20$ (< 0.30 at the onset of r-processing) are required to account for the 3rd r-process peak formation ($A = 195$). Notable is that the "envelope" made by the curves for various Y_{e0} reasonably fits the solar r-process distribution. This implies that the wide range of Y_e (in terms of space and time) in the presented case leads to production of all the heavy r-process nuclei.

4. Summary

Using ejecta-mass tracers from a self-consistent 2D explosion model and wind trajectories from a semi-analytic black hole wind model, we computed the nucleosynthesis in the early ejecta

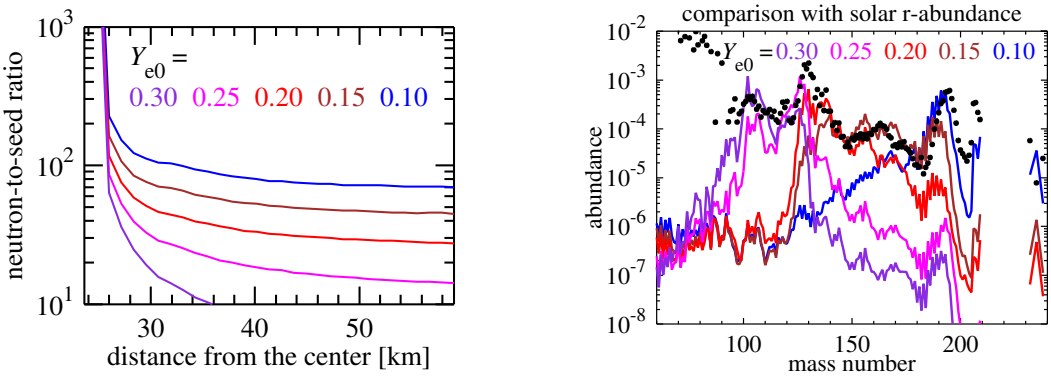

Figure 8: Left: Neutron-to-seed ratios at the onset of r-processing (2.5×10^9 K) as a function of the distance from the center for various initial electron fractions ($Y_{e0} = 0.10$, 0.15, 0.20, 0.25, and 0.30). Right: Mass-averaged nucleosynthetic yields for various initial electron fractions (lines), which are compared with the solar r-process distribution (dots).

of ECSNe and in the neutrino-driven ejecta of black hole accretion tori. Our results are summarized as follows (see [14] for more detail).

The n-rich lumps in the early ECSN ejecta with Y_e down to 0.4, which are absent in more massive CCSNe, allow for a sizable production of the elements from Zn to Zr in NSE and by the α-process (not by the r-process). The model yields Ge, Sr, Y, and Zr in very good agreement with abundances of r-process deficient Galactic halo stars. A mild reduction of the minimum Y_e to $\sim$0.30–0.35, which cannot be excluded due to limited numerical resolution and the lack of the third dimension, leads to a weak r-process up to the silver region (Pd, Ag, and Cd), again well matching these elements in r-process deficient stars. The formation of heavy r-process nuclei requires Y_e to be as low as $\sim$0.15–0.20 and seems out of reach for our models.

Our model of black hole winds suggests that the innermost wind trajectories attain substantially higher entropies ($> 100 k_B$ per nucleon) and shorter expansion timescales (< 10 ms). This indicates that all the relevant astrophysical conditions, i.e., NS-NS and BH-NS mergers and collapsars (or hypernovae) are potential factories of the heavy r-process nuclei. However, our nucleosynthesis result shows that significant neutron-richness in the wind is still required in order to account for the formation of the 3rd r-process peak. In this regard, NS-NS and BH-NS are favored compared to collapsars, since the accretion tori originate from neutron-star matter (and moreover, $L_{\bar{\nu}_e} > L_{\nu_e}$) in the former case and iron-peak (or alpha) elements in the latter, respectively.

DFG grants EXC153, SFB/TR27, and SFB/TR7, and computing time at the NIC in Jülich, HLRS in Stuttgart, and the RZG in Garching are acknowledged.

References

[1] Woosley, S. E., Wilson, J. R., Mathews, G. J., Hoffman, R. D., & Meyer, B. S. 1994, *Astrophys. J.*, 433, 229

[2] Takahashi, K., Witti, J., & Janka, H.-T. 1994, *Astron. Astrophys.*, 286, 857

[3] Qian, Y. -Z. & Woosley, S. E. 1996, *Astrophys. J.*, 471, 331

[4] Otsuki, K., Tagoshi, H., Kajino, T., & Wanajo, S. 2000, *Astrophys. J.*, 533, 424

[5] Wanajo, S., Kajino, T., Mathews, G. J., & Otsuki, K. 2001, *Astrophys. J.*, 554, 578

[6] Thompson, T. A., Burrows, A., & Meyer, B. S. 2001, *Astrophys. J.*, 562, 887

[7] Wanajo, S., Tamamura, M., Itoh, N., Nomoto, K., Ishimaru, I., Beers, T. C., & Nozawa, S. 2003, *Astrophys. J.*, 593, 968

[8] Ning, H., Qian, Y. -Z., & Meyer, B. S. 2007, *Astrophys. J.*, 667, L159

[9] Kitaura, F. S., Janka, H. -Th., & Hillebrandt, W. 2006, *Astron. Astrophys.*, 450, 345

[10] Janka, H. -Th., Müller, B., Kitaura, F. -S., & Buras, R. 2008, *Astron. Astrophys.*, 485, 199

[11] Hoffman, R. D., Müller, B., & Janka, H.-T. 2008, *Astrophys. J.*, 676, L127

[12] Wanajo, S., Nomoto, K., Janka, H.-T., Kitaura, F. S., Müller, B. 2009, *Astrophys. J.*, 695, 208

[13] Hüdepohl, L., Müller, B., Janka, H.-Th., Marek, A., Raffelt, G. G 2010, *Phys. Rev. Lett.*, 104, 251101

[14] Wanajo, S., Janka, H.-T., & Müller, B. 2010, *Astrophys. J.*, submitted; arXiv1009.1000

[15] Ruffert, M. & Janka, H.-T. 1998, *Astron. Astrophys.*, 344, 573

[16] Janka, H.-T., Eberl, T., Ruffert, M., & Fryer, C. L. 1999, *Astrophys. J.*, 527, L39

[17] Lattimer, J. M., Mackie, F., Ravenhall, D. G., & Schramm, D. N. 1977, *Astrophys. J.*, 213, 225

[18] Meyer, B. S. 1989, *Astrophys. J.*, 343, 254

[19] Freiburghaus, C., Rosswog, S., & Thielemann, F.-K. 1999, *Astrophys. J.*, 525, L121

[20] Goriely, S., Demetriou, P., Janka, H. -Th., Pearson, J. M., & Samyn, M. 2005, *Nucl. Phys. A*, 758, 587

[21] Surman, R., McLaughlin, G. C., Ruffert, M., Janka, H. -Th., & Hix, W. R. 2008, *Astrophys. J.*, 679, L117

[22] Setiawan, S., Ruffert, M., & Janka, H. -Th. 2006, *Astron. Astrophys.*, 458, 553

[23] Ishimaru, Y., Wanajo, S., & Prantzos, N. 2010, in this volume

[24] De Donder, E. & Vanbeveren, D. 2004, *New Astron. Rev.*, 48, 861

[25] Lattimer, J. M., & Swesty, F. D. 1991, *Nucl. Phys. A*, 535, 331

[26] Nomoto, K. 1987, *Astrophys. J.*, 322, 206

[27] Honda, S., Aoki, W., Ishimaru, Y., Wanajo, S., & Ryan, S. G. 2006, *Astrophys. J.*, 643, 1180

[28] Wanajo, S. 2006, *Astrophys. J.*, 650, L79

[29] Cowan, J. J., et al. 2005, *Astrophys. J.*, 627, 238

[30] Roederer, I. U., Sneden, C., Lawler, J. E., & Cowan, J. J. 2010, *Astrophys. J.*, 714, L123

[31] Sneden, C., et al. 2003, *Astrophys. J.*, 591, 936

[32] Poelarends, A. J. T., Herwig, F., Langer, N., & Heger, A. 2008, *Astrophys. J.*, 675, 614

[33] Woosley, S. E. & Hoffman, R. D. 1992, *Astrophys. J.*, 395, 202

[34] Hartmann, D., Woosley, S. E., & El Eid, M. F. 1985, *Astrophys. J.*, 297, 837

[35] Wanajo, S. & Ishimaru, I. 2006b, *Nucl. Phys. A*, 777, 676